EDGEWOOD CHEMICAL BIOLOGICAL CENTER
U.S. ARMY RESEARCH, DEVELOPMENT AND ENGINEERING COMMAND
Aberdeen Proving Ground, MD 21010-5424

ECBC-TR-1212

# STOCHASTIC RADIATIVE TRANSFER MODEL FOR CONTAMINATED ROUGH SURFACES: A FRAMEWORK FOR DETECTION SYSTEM DESIGN

**Avishai Ben-David**

**RESEARCH AND TECHNOLOGY DIRECTORATE**

**Charles E. Davidson**

**SCIENCE AND TECHNOLOGY CORPORATION**
**Edgewood, MD 21040-2734**

**November 2013**



U.S. ARMY RDECOM

Disclaimer

The findings in this report are not to be construed as an official Department of the Army position unless so designated by other authorizing documents.

# REPORT DOCUMENTATION PAGE

*Form Approved*
*OMB No. 0704-0188*



| **1. REPORT DATE** *(DD-MM-YYYY)* | **2. REPORT TYPE** | **3. DATES COVERED** *(From - To)* |
|---|---|---|
| XX-11-2013 | Final | Jan 2013 - Sep 2013 |

**4. TITLE AND SUBTITLE**
Stochastic Radiative Transfer Model for Contaminated Rough Surfaces: A Framework for Detection System Design

**5a. CONTRACT NUMBER**

**5b. GRANT NUMBER**

**5c. PROGRAM ELEMENT NUMBER**

**6. AUTHOR(S)**
Ben-David, Avishai (ECBC); and Davidson, Charles E. (STC)

**5d. PROJECT NUMBER**

**5e. TASK NUMBER**

**5f. WORK UNIT NUMBER**

**7. PERFORMING ORGANIZATION NAME(S) AND ADDRESS(ES)**
Director, ECBC, ATTN: RDCB-DRD-P, APG, MD 21010-5424
STC, 500 Edgewood Road, Suite 205, Edgewood, MD 21040-2734

**8. PERFORMING ORGANIZATION REPORT NUMBER**
ECBC-TR-1212

**9. SPONSORING / MONITORING AGENCY NAME(S) AND ADDRESS(ES)**
U.S. Army Edgewood Chemical Biological Center, Aberdeen Proving Ground, MD 21010-5424

**10. SPONSOR/MONITOR'S ACRONYM(S)**
ECBC

**11. SPONSOR/MONITOR'S REPORT NUMBER(S)**

**12. DISTRIBUTION / AVAILABILITY STATEMENT**
Approved for public release; distribution is unlimited.

**13. SUPPLEMENTARY NOTES**

**14. ABSTRACT-LIMIT 200 WORDS**

We developed a framework to evaluate the performance of a detection system for contaminated surfaces. We employed the radiative transfer model for contaminated surfaces (Ben-David and Davidson, ECBC-TR-1084, 2013) and transformed the physical model into a stochastic probability model with which detection probability and false alarms can be estimated for scenarios of interest. Our algorithm employs a data fusion approach known as a distributed binary integration system (also known as a double-threshold detector, or *m*-out-of-*n* detector) in order to combine the individual detection results from multiple scans over several potentially contaminated areas. With our probability model we can explore the parameter space (e.g., number of measurements, time to detect, area to monitor, sparsity of the contamination, field of view, etc.) and study the tradeoffs between parameters that affect the overall system detection performance. We can also use the stochastic model to set sensor requirements for a contamination scenario. We presented plots that demonstrate the interaction between parameters and an example for the detection of a potassium chlorate contaminated "car" with a $CO_2$ tunable laser system.

**15. SUBJECT TERMS**

| | | |
|---|---|---|
| Radiative transfer | Contaminated surfaces | Detection |
| Rough surface | BRDF | Reflectance |
| Fill factor | CFAR | Data fusion |

(Continued on next page.)

| **16. SECURITY CLASSIFICATION OF:** | | | **17. LIMITATION OF ABSTRACT** | **18. NUMBER OF PAGES** | **19a. NAME OF RESPONSIBLE PERSON** |
|---|---|---|---|---|---|
| **a. REPORT** | **b. ABSTRACT** | **c. THIS PAGE** | | | Renu B. Rastogi |
| U | U | U | UU | 42 | **19b. TELEPHONE NUMBER** *(include area code)* (410) 436-7545 |

SF 298 Block 15. Subject Terms (Continued)

Distributed binary integration
Distributed sensor system
Double-threshold detector
*m*-out-of-*n* detector
Potassium chlorate
Probability theory
System performance
Probability of detection and false alarm

# PREFACE

The work described in this report was started in January 2013 and completed in September 2013.

The use of either trade or manufacturers' names in this report does not constitute an official endorsement of any commercial products. This report may not be cited for the purposes of advertisement.

The text of this report is published as received and was not edited by the Technical Releases Office, U.S. Army Edgewood Chemical Biological Center.

This report has been approved for public release.

Blank

## TABLE OF CONTENTS



## LIST OF FIGURES

# Stochastic radiative transfer model for contaminated rough surfaces: a framework for detection system design

**Avishai Ben-David**
*RDECOM, Edgewood, Chemical Biological Center, Aberdeen Proving Ground, MD 21010*
*e-mail: avishai.bendavid@us.army.mil*

**Charles E. Davidson**
*Science and Technology Corporation, Edgewood, MD 21040*
*e-mail: charles.e.davidson2.ctr@us.army.mil*

**Abstract**
We developed a framework to evaluate the performance of a detection system for contaminated surfaces. We employ the radiative transfer model for contaminated surfaces (Ben-David and Davidson, ECBC-TR-1084, 2013) and transform the physical model into a stochastic probability model with which detection probability and false alarms can be estimated for scenarios of interest. Our algorithm employs a data fusion approach known as a distributed binary integration system (also known as a double-threshold detector, or *m*-out-of-*n* detector) in order to combine the individual detection results from multiple scans over several potentially contaminated areas. With our probability model we can explore the parameter space (e.g., number of measurements, time to detect, area to monitor, sparsity of the contamination, field of view, etc.) and study the tradeoffs between parameters that affect the overall system detection performance. We can also use the stochastic model to set sensor requirements for a contamination scenario. We presented plots that demonstrate the interaction between parameters and an example for the detection of a potassium chlorate contaminated "car" with a $CO_2$ tunable laser system.

**Subject Terms** Radiative transfer, contaminated surfaces, detection, rough surface, BRDF, reflectance, fill factor, distributed binary integration, CFAR, data fusion, distributed sensor system, double-threshold detector, *m*-out-of-*n* detector, potassium chlorate, probability theory, system performance, probability of detection and false alarm.

## 1. Introduction

In a recent publication[1] we have developed a radiative transfer model with which we addressed long-wave infrared (LWIR) passive and active spectral reflectance measurements of potassium chlorate or ammonium nitrate contaminated rough surfaces. The radiative transfer model was developed from physics-based principles with the aid of empirical approximation of the uncontaminated rough surface reflectance. In this report our objective is to develop a framework for the radiative transfer model where the parameters are allowed to be stochastic (i.e., fluctuate) and thus the new model will be able to predict the performance of a notional system with traditional figures of merit: probabilities of detection and false alarm. In this report

we only address an active infrared laser system (pulsed or continuous wave) that probes the contaminated surface and measures the reflectance at the specular reflectance angle (e.g., a bi-static lidar system) or at the backscatter angle. In future reports we will enlarge the framework to passive remote sensing where the reflected thermal radiation and for a Raman system that is used to interrogate contaminated rough surfaces.

The main steps in developing a framework for stochastic radiative transfer model are:

I. Identifying the relevant physical parameters to become stochastic random variables (RV).
II. Choosing probability models for the selected RVs.
III. Combining the RVs with the physical radiative transfer model into a probability model for the measured (predicted) signal.
IV. Selecting a signal processing method with which spectral signal is transformed to a detection score.
V. Applying data acquisition constraints to the detection scenario: time to detect, surface area to cover.
VI. Determine system-level performance: combining many single (local) measurement probabilities of detection and false alarm into a scenario (global) probability of detection and false alarm.

## 2. Overview

We start by giving a brief overview of a practical scenario for which we envision the implementation of our stochastic model. A suspected car at a check-point is scanned with a LWIR laser beam and reflected signals are measured throughout key areas of the suspected car. Within a given time and after many measurements are acquired–where each measurement is a vector with $p$ spectral bands–a detection score is broadcasted by the algorithm. The detection score is evaluated with respect to a probability of false alarm (the car is falsely declared as "contaminated") and the probability of missed detection (equal to one minus the probability of detection) where the car is contaminated but the detection algorithm did not broadcast the proper "contamination detected" declaration. The parameters "missed detection" and "false alarm" drive the detection algorithm in opposite directions; when the former decreases the later increases. In the scenario of a suspected car we are willing to endure higher false alarm rates in order to minimize the chance of a missed detection, because we assume false alarms will only necessitate a secondary (e.g., manual) investigation of the car at the check-point location.

The basic radiative transfer model [Eq. 10, in reference 1] for the reflected signal from a contaminated surface, illuminated at incidence angle $\theta_i$ and measured at reflectance angle $\theta$ is given by

$$\begin{cases} R(\theta,\theta_i) = (1-f)\times R_0 + f\times\left( R_t + (1-R_t)R_0 \times e^{-h\left(\frac{1}{\cos(\theta_i)}+\frac{1}{\cos(\theta)}\right)(\alpha+g\Delta n)} \right) \\ R_0 = \rho_0 \exp(a_0\lambda^{-2} + b_0\lambda^{-1} + c_0) \\ R_t = \rho_t \exp(a_t\lambda^{-2} + b_t\lambda^{-1} + c_t) \end{cases} \quad (1)$$

where, $f$ is the fill factor of the contaminated area (the fraction of illuminated spot that is contaminated), $h$ is the contamination thickness (e.g., modeled as a film), $R_0(\theta,\theta_i)$ is rough surface reflectance from the car, $R_t(\theta,\theta_i)$ is the reflectance of the contamination (i.e., target material) modeled as a rough surface due to morphology of the contamination, $\theta_i$ and $\theta$ are the incident and reflected angles measured counter-clockwise from the surface's normal (i.e., for specular reflectance geometry $\theta = -\theta_i$, and for lidar backscatter geometry $\theta = \theta_i$), $\alpha$ is the spectral absorption coefficient, and $g\Delta n$ is a dispersion correction to $\alpha$. In (1), top line, $R_0$, $R_t$, and $R$ are wavelength dependent (wavelength dependence, $\lambda$, is omitted for clarity); $f$, $h$, $a$, $b$, $c$, are all scalars. Both $R_0$ and $R_t$ are given with empirical coefficients ($a$, $b$, $c$) and the spectral Fresnel reflectance coefficients $\rho_0$ and $\rho_t$ are computed at incidence angle $\theta_i$. In [1] we showed very good results of applying the model (2) for specular geometry. In this report we speculate that also for lidar backscatter geometry (that can be implemented with a hand-held sensor) the model given by (2) provides good results.

Thus, given atmosphere with transmission $t_{atm}(range)$ where range is the folded path from the source to the surface and back to the detector an illuminating source with constant strength $L_{source}(\theta_i)$ at a distance from the surface (distance $r_{source}$) and a detector at a distance $r_{\text{detector}}$ and angle $\theta$ from the surface, the measured reflected signal is given by

$$M_{\text{detector}}(\theta) = L_{source}(\theta_i)\frac{t_{atm}}{(r_{source}+r_{\text{detector}})^2} R(\theta_i,\theta) = K_{system}\times R(\theta,\theta_i) \quad (2)$$

where $K_{system} = L_{source}(\theta_i)t_{atm}(r_{source}+r_{\text{detector}})^{-2}$ is a system constant (for a given geometry) and $R(\theta,\theta_i)$ is given in Eq. (1).

To develop a probability model for $M_{\text{detector}}$ we need to develop (or assume) a statistical model for all random variables (RV) in the model equation and then modify the statistics of $R(\theta,\theta_i)$ with the scaling factor $K_{system}$. If needed, one can regard $K_{system}$ as a RV (e.g., due to fluctuations in atmospheric transmission or laser power) – in this work (for simplicity) $K_{system}$ is not a RV. The objective is to develop a probability density function (*pdf*) for the at-aperture signal $M_{\text{detector}}$, and use it in a detection algorithm (e.g., a matched filter detector) to produce detection scores that can be evaluated for probability of detection, probability of false alarm, and

probability of missed detection. In finding probability model for the RVs in (2) we strive for a balance between complexity of the statistical description and ease of use at the expense of accuracy. It is counterproductive to describe RVs with complex mathematical functions that we cannot use when we need to manipulate RVs in the form of multiplications and additions of RVs that lead to the *pdf* of (2).

The RVs that we address in this study are the fill factor *f*, contamination thickness *h*, rough surface reflectance $R_0$, and the reflectance of the contaminated target, $R_t$. The statistics of the fill factor *f* is affected by the field of view (FOV), the cross-sectional area distribution $\varphi_a(a)$ of the contamination, and the total mass of the contamination per unit area. The spill area-distribution $\varphi_a(a)$ is the footprint distribution of the contamination on the surface. While $\varphi_a(a)$ is related to the intrinsic diameter distribution function $\Phi_{diameter}(diameter)$ of the contamination particles, the two are not the same. The spill-distribution $\varphi_a(a)$ describes the interaction between single particles due to conglomeration, clumping, how particles fall out (spill) of a sack that moved by a car, etc., whereas $\Phi_{diameter}(diameter)$ is the size distribution of the individual particles before they were spread (spilled) on the surface (e.g., a size distribution of a powder before it was put in a sack). The contamination footprint cross-sectional area distribution $\varphi_a(a)$ is used to compute the *pdf* for *f*, $P_f(f)$. The particle size distribution function $\Phi_{diameter}(diameter)$ may be used to compute the *pdf* of the target thickness *h*, $P_h(h)$, when one assumes a single layer of particles on the surface for which $h \cong diameter$. In this work we regard the *pdf*s for *f* and *h* to be independent of each other (for convenience and because we do not know the mechanism of spillage that create *f* and *h*), however, if one choose to impose dependency between *f* and *h*, then a bivariate $P_{h,f}(h,f)$ can be used (a bivariate *pdf* for two marginal normals is easily obtained, and for non-normal the concept of copula can be employed). In the notation for a general *pdf*, e.g., $P_y(x \mid z)$, the subscript denotes the parameter (*y*) for the *pdf* and in parentheses it is a dummy argument (*x*). The notation $x \mid z$ reads as *x* conditional to a given *z* value; $P_y(x)$ denotes an unconditional *pdf*.

Let's assume that we are able to derive the *pdf* $P_R(R)$ for the measured reflectance *R* in (1); then with a simple transformation the *pdf* of (2) is $P_M(M) = K_{sustem}^{-1} P_R(M / K_{system})$. With $P_M(M)$ we can formulate our binary Neyman-Pearson hypothesis testing[2] regarding the data *M* under $H_0$ and $H_1$ scenarios, where for the null hypothesis $H_0$ the interpretation is that the data does not contain the signal of interest (e.g., a target), and the alternative hypothesis $H_1$ is that the data does contain the signal of interest in addition to noise and interferences. Under the two hypotheses

$$\begin{Bmatrix} M \mid H_0 = M(fh = 0) \\ M \mid H_1 = M(fh \neq 0) \end{Bmatrix}. \quad (3)$$

The fluctuations in *M* are due to both additive noise (whose source can be—but not limited to—detector noise), and to multiplicative noise (e.g., due to clutter). In most sensors system noise is small, and most of the noise is due to clutter which in our model is represented by the uncontaminated rough surface *pdf* $P_{R_0}(R_0)$.

Analyzing detection performance requires selecting a signal processing method with which to determine the presence of the target signals in the data. We have chosen the standard matched filter algorithm, which is optimal for additive Gaussian noise. Although our problem is not described by a simple additive model (and thus the matched filter is not optimal), the matched filter is a standard technique used as a benchmark for comparing algorithms, leads to convenient performance analysis, and is therefore a suitable choice. The matched filter detection score is given by

$$score = \frac{[M - E(M \mid H_0)]^T \operatorname{cov}(M \mid H_0)^{-1} \delta}{\delta^T \operatorname{cov}(M \mid H_0)^{-1} \delta} \quad (4)$$

where $E(\cdot)$ is a mean (expectation), $\operatorname{cov}(\cdot)$ is a covariance operation, superscript "*T*" is a matrix transpose operation (when *M* is a column spectral vector of measurements with *p* spectral bands and $M^T$ is a row vector), $\delta$ is the target spectral vector that represent the spectral direction of the intrinsic contamination (to be discussed in section 5). The simplest, but not necessarily best, choice for $\delta$ is the spectral absorption coefficient $\alpha$ in (1). For the detection scores we compute a probability of detection $P_{\text{detect}}$ and probability of false alarm $P_{\text{false-alarm}}$. The scores in (4) are function of the $H_0$ condition, namely, a function of the local rough surface properties. Thus, it is prudent to assume that different parts of the suspected car will have different $H_0$ signals (e.g., due to non-uniformity of materials, and geometry of orientation with respect to incidence angle). In the general detection case we have $J_{AOR}$ areas of regard (AOR) in the suspected car, each area of regard produces $N_{scores}$. The scores for each $J_{AOR}$ are characterized by $P_{\text{detect}}$ and $P_{\text{false-alarm}}$. We combine the $J_{AOR} \times N_{scores}$ local scores and probabilities into one (global) set of probabilities, $P_{\text{detect}}(car)$ and $P_{\text{false-alarm}}(car)$ with the "binary integration" method[3, 4], a method that is used in radar detection algorithms. The number of AORs can be set according to distinct areas that affect the substrate reflectivity $R \mid H_0$: the number of different materials of the uncontaminated car's surfaces (e.g., rubber, aluminum, painted aluminum, etc.), and/or the orientation of the surfaces (e.g., horizontal hood and trunk, vertical doors), and could also depend on a priori information regarding the likelihood of different areas of the car to be contaminated.

The total number of detection scores $J_{AOR} \times N_{scores}$ is a function of external constraints such as total time (*T*) available for scanning a suspected car, sensor acquisition rate (laser pulse repetition frequency, *PRF*, for an active sensor), and the sensor field of view (solid angle, *FOV* in steradians) whose viewing area is $r_{source}^2 FOV$. For convenience, we assume that the laser beam divergence matches the field of view, hence, $r_{source}^2 FOV$ is the illuminated spot-area on the

contaminated surface. The internal relationship between the external constraints and a simple flowchart is given by

$$\left\{\begin{array}{l}\text{external}\\ \text{constraints}\\ J_{AOR}\times N_{scores}=T\times PRF\\ N_{scores}=\dfrac{A/J_{AOR}}{r_{source}^2 FOV}\end{array}\right\}\rightarrow\left\{\begin{array}{l}\text{detector}\\ \text{signal}\\ M\mid H_0\\ M\mid H_1\end{array}\right\}\rightarrow\left\{\begin{array}{l}\text{detection}\\ \text{scores}\\ score(J_{AOR}\times N_{scores})\\ P_{\text{detection}}(J_{AOR})\\ P_{\text{false-alarm}}(J_{AOR})\end{array}\right\}\rightarrow\left\{\begin{array}{l}\text{overall}\\ \text{probability}\\ P_{\text{detection}}(car)\\ P_{\text{false-alarm}}(car)\end{array}\right\} \quad (5)$$

Note that in (5) $A$ is the sum of the viewed areas for each $J_{AOR}$ areas of regard, $A=\sum_{j=1}^{J}A_j$, $N_{scores}$ is the number of measurements for *each* area of regard that is collected with a sensor with a given $FOV$ (*sr*), and that $p$ spectral bands are collected every $PRF^{-1}$ seconds. The illuminated area (by the active source) for a single laser shot on the contaminated surface is $r_{source}^2 FOV$. Solid angle $FOV$ (*sr*) is the square of the linear FOV in radians. In (5) each of the AORs contains $N_{scores}$, however, one can allow a different number of measurements for each $j$, $N_j$, and that $J_{AOR}\times N_{scores}=\sum_{j=1}^{J}J_j N_j$. The sensor can be a single pixel detector or an array for which the acquisition of $N_{scores}$ may take less time. For example, for $N$=100, $J$=6, and $T$=30s, the $PRF=J\times N/T=20\,Hz$, which implies that a vector with $p$ spectral bands must be acquired every $5ms$ – a difficult task not to be underestimated. With the snapshot-advantage architecture[5] (see Fig. 1 in reference 5) this task can be achieved; one can have a detector with $x$-by-$y$-by-λ data cube where $x=y=\sqrt{N}$, and λ =$p$, that is acquired simultaneously for each of the $J$ areas of regard. In order for an active sensor to take advantage of the snapshot-advantage architecture (i.e., an imaging receiver) one would need multiple sources or else ensure that the illuminated spot size is large enough to illuminate each pixel in the image simultaneously. In this report we assume that $N$ and $J$ are the external parameters to the global probability model and we gloss over the acquisition strategy that was employed to obtain them.

### 3. Probability model for stochastic variables

We describe the options for the principal RVs and our choice for a statistical model. When selecting a statistical model for a RV we consider the range of the RV: e.g., the support range for contamination thickness, $h$, is zero to infinity or zero to $h_{\max}$; the support range for a fill factor, $f$, is zero to one. There is more than one *pdf* that can describe the range of values of a given RV. The most likely choice for a *pdf*, in the absence of any prior knowledge, is a *pdf* whose entropy is a maximum. For example, given a RV $x$ that is known to exist only within a limited range (support) $x_1\le x\le x_2$ and is zero outside the interval $[x_1,x_2]$ the most likely *pdf* is a uniform *pdf*, i.e., with our maximum ignorance we must accept that all values $x_1\le x\le x_2$ are equally likely. If

we have prior knowledge about $x$ that the mean $E(x) > 0$, and the support $0 \le x \le \infty$, then an exponential *pdf* is the most likely *pdf* for $x$; If we know the mean $E(x)$ and variance $V(x)$ of $x$, then the normal distribution for which $-\infty \le x \le \infty$ is the most likely *pdf*.

In this study we assume measurements are collected at $p$ wavelengths, hence, $R_0$, $R_t$, and $M$ are multivariate RVs (i.e., $p$-by-1 vectors), whereas $f$ and $h$ are univariate RVs (i.e., 1-by-1 scalars).

### 3.1 *Surface roughness $R_0$ and $R_t$*

The RV for surface roughness $R_0 = \rho_0 \exp(a_0\lambda^{-2} + b_0\lambda^{-1} + c_0) = \rho_0 D$ where $D = \exp(a_0\lambda^{-2} + b_0\lambda^{-1} + c_0)$ is the decay function (see equation 3 in reference 1) contains three RVs, $-\infty \le (a_0, b_0, c_0) \le \infty$ and is bounded in the support range $0 \le R_0 \le 1$. If we knew the means $(\mu_{a0}, \mu_{b0}, \mu_{c0})$ and the variances $(\sigma_{a0}^2, \sigma_{b0}^2, \sigma_{c0}^2)$ of $(a_0, b_0, c_0)$; we can assume a normal distribution, $N(\mu, \sigma^2)$, as the most likely *pdf* for $(a_0, b_0, c_0)$, and $R_0$ is given by lognormal *pdf*, $LN(\mu, \sigma^2)$ as

$$\left.\begin{aligned} &R_0 \sim LN(\ln(\rho_0) + \mu_D, \Sigma_D) \\ &\mu_D = \mu_{a0}\lambda^{-2} + \mu_{b0}\lambda^{-1} + \mu_{c0} \\ &\Sigma_D = \sigma_{a0}^2(\lambda^{-2})(\lambda^{-2})^T + \sigma_{b0}^2(\lambda^{-1})(\lambda^{-1})^T + \sigma_{c0}^2\mathbf{1}\mathbf{1}^T \\ &D \sim LN(\mu_D, \Sigma_D) \end{aligned}\right\} \quad (6)$$

where $\mathbf{1}$ is a $p$-by-1 vector with all ones. Note, that in (6) we did not enforce the upper bound constraint $R_0 \le 1$ (the lower bound is assured to be greater than zero when using lognormal *pdf*). Nevertheless, since we know from lab experiments that $D \sim LN(\mu_D, \Sigma_D)$ is spectrally smooth function due to the spectral dependence imposed by the 2nd order polynomial $a_0\lambda^{-2} + b_0\lambda^{-1} + c_0$, we can choose scalar values for $(a_0, b_0, c_0)$ to obtain a reasonable decay function $D$, and furthermore we can ensure that our choice for $(\mu_D, \Sigma_D)$ will produce a physical rough surface reflectance $R_0 \le 1$. The same can be done to produce a *pdf* for the contamination (viewed as a rough surface) $R_t$ using $(a_t, b_t, c_t)$,

$$\left.\begin{aligned} &R_t \sim LN(\ln(\rho_t) + \mu_{Dt}, \Sigma_{Dt}) \\ &\mu_{Dt} = \mu_{at}\lambda^{-2} + \mu_{bt}\lambda^{-1} + \mu_{ct} \\ &\Sigma_{Dt} = \sigma_{at}^2(\lambda^{-2})(\lambda^{-2})^T + \sigma_{bt}^2(\lambda^{-1})(\lambda^{-1})^T + \sigma_{ct}^2\mathbf{1}\mathbf{1}^T \\ &D_t \sim LN(\mu_{Dt}, \Sigma_{Dt}) \end{aligned}\right\} \quad (7)$$

In future work we may generalize (6, 7) and treat the Fresnel reflectance $\rho_0$ and $\rho_t$ as RVs, which would model a change in composition of the car's surface and the target.

### 3.2 *Contamination thickness h*

In our physical model the thickness *h* of the contamination is an average value across the contaminated areas within the field of view. Due to the non-uniformity of contamination we expect variations in *h*, hence fluctuations in the transmission $t \propto \exp(-\alpha h)$ through the contamination. Our first option is a uniform *pdf* for *h*. We can assume that in practice *h* is bounded, $h_{\min} \le h \le h_{\max}$, where $h_{\max}$ is chosen such that the transmission $t \propto \exp(-\alpha h)$ is practically zero (i.e., within sensor noise). A uniform *pdf* for $0 \le h \le h_{\max}$ has maximum entropy and thus is advantageous (maximum entropy implies high likelihood of occurance). However, the *pdf* of transmission (easily obtained with transformation of variables for the *pdf* of *h*) will have higher occurrence for low transmission than high transmission, a scenario that we do not think as being reasonable. On the contrary, we think that most transmission events across the contaminated surface will be of high value (i.e., associated with small *h*). Our second choice is an exponential *pdf* for *h*. We know that $h>0$ and thus (for maximum entropy) we are tempted to choose an exponential *pdf* for $0 \le h \le \infty$, hence larger probability for small contamination (thin layer *h*) than for large amount of contamination. The problem with exponential *pdf* for *h* is its high non-zero density for $h=0$ and thus the exponential choice imposes restriction on the interpretation of the $H_1$ scenario (contamination is present), i.e., $P_h(h=0|H_1) = 0$ is required by definition of $H_1$. Our third option is a simple linear *pdf*, $pdf(h) \propto const / h$ for *h* between $h_{\min} \le h \le h_{\max}$ such that $pdf(h_{min}) > pdf(h_{max})$ (an additional information to set the slope of the *pdf* is required) and hence the *pdf* of the transmission will have higher occurrence for small *h* than for large *h* (the behavior we desire). Other options for *pdf*s are the use of complex (but flexible) functions such as *beta* and *gamma pdf*s that can be constrained (with additional information) to give the expected behavior for the *pdf*s of *h* and the transmission. If we have information about the size distribution $\Phi_{diameter}(diameter)$ of the particles, we can use it to form a *pdf* for *h*. For example, we can assume that the contaminated surface is composed of a *single layer* of particles, and thus, the thickness is proportional to a diameter. Thus, the *pdf* of *h* will have a similar shape as the particle size distribution. The experimental data[6] suggests that a monolayer of contamination is reasonable. Our, choice for *pdf* for *h* is to use the size distribution $\Phi_{diameter}(diameter)$ or if is not available to use the simple linear $pdf(h) \propto const / h$, for *h* between $h_{\min} \le h \le h_{\max}$, that is, $P_h(h) = 2\dfrac{h_{\max} - h}{(h_{\max} - h_{\min})^2}$, which has a mode at $h_{\min}$ and zero density at $h_{\max}$.

### 3.3 *Contamination fill factor f*

A *pdf* for *f* was not given in the MIT-LL report[6]; only the footprint cross-sectional area of the spill distribution $\varphi_a(a)$ was given. Thus, we had to compute the *pdf* for the fill factor. We

compute $P_f(f)$ with two methods: via simulations and with a theory (see Appendix A for details of the simulation method). A brief description of the two methods is as follows.

(1) a $P_f(f)$ is computed with a simulation program where we construct a random surface populated with random cross-sectional footprints that are sampled from $\varphi_a(a)$ and are uniformly distributed on a surface. The footprints are not allowed to intersect (i.e., no overlap between footprints). With this complex simulation we compute a fill factor for a given field of view by moving the *FOV* over the simulated random surface (a digital image) and computing the area of all the particles in the simulations. Due to pixilation of the objects in the digital image (the size of *FOV* and the spill footprint) the computed $P_f(f)$ may contain sharp spikes; therefore, we typically smooth the *pdf*.

(2) We compute a $P_f(f)$ with a theoretical method where the location of the contamination sites are located at random locations[7] based on random theory of distribution of random centers in a hyper volume (for our application we reduced the volume to a surface). The spill footprint sizes are sampled from $\varphi_a(a)$. The probability of intersection between a given footprint (modeled as a circle) and the edge of the *FOV* (modeled as a rectangle) is computed. The theoretical method is based on detailed geometrical calculations for intersection of shapes (*FOV* and footprint); it utilizes approximations that are only valid under certain conditions.

At present, we choose to use the simulation program to produce fill factor probability. In future work we intend to improve the accuracy of the theoretically derived *pdf*.

The prior probability $P(H_1)$ for $H_1$ event (i.e., the likelihood that the contamination will be present within an *FOV*) can be easily computed in the simulation by the ratio of number of FOVs that *are not* empty (i.e., *FOV*s that contain any target material) to the number of FOVs that are contained in the AOR. For example, if the *FOV* is 10 *mr*, AOR is 1 $m^2$, and the distance to the AOR is 10*m*, then the number of independent *FOV*s is $1m^2/[10mr \times 10]^2 = 100$. If in the simulation only, say, 5 *FOV*s contain the target, then $P(H_1) = 5/100$. The prior probability $P(H_1)$ is dependent on the surface density of the contamination, the cross-sectional area distribution $\varphi_a(a)$, and the size of the FOV.

### 4. *Statistics of the signal M*

It is extremely difficult to derive the *pdf* of $M_{\text{detector}}$ in (2). Our approach is to compute the moments of $M_{\text{detector}}$ and then to fit an analytical *pdf* to the computed moments. Our goal is to obtain a *pdf* for the detection scores (4) from which we compute a probability of detection and false alarm. Given the physical model (2) $M_{\text{detector}} = K_{system} \times R(\theta)$ we compute its $n^{\text{th}}$ moment

$$E(M^n) = K_{system}^n E[R^n(\theta)] \quad (8)$$

By carefully expanding $R^n(\theta)$ of (2) we obtain a long series of terms that is an $n^{\text{th}}$ order polynomial with the RVs (*f*, *exp(-h),* $R_t$ , and $R_0$) where each term of the series is of the form $f^{n_f} \exp(-h)^{n_h} R_t^{n_{Rt}} R_0^{n_{R0}}$ where the sum of the exponents $n_f + n_h + n_{Rt} + n_{R0} = n$. If we assume that the RVs are statistically independent, the expectation of $f^{n_f} \exp(-h)^{n_h} R_t^{n_{Rt}} R_0^{n_{R0}}$ is simply given by $E(f^{n_f} \exp(-h)^{n_h} R_t^{n_{Rt}} R_0^{n_{R0}}) = E(f^{n_f})E(\exp(-h)^{n_h})E(R_t^{n_{Rt}})E(R_0^{n_{R0}})$ where each of the expectations can be computed with the proper statistical model chosen for that specific RV.

With first and second moments (*n*=1 and *n*=2) we can approximate the *pdf* of *M* as multivariate normal (for *p* spectral bands) $M \sim N(\mu_M, \sum_M)$, or a lognormal $M \sim LN(\mu_M, \sum_M)$, where the population parameters are

$$\left\{ \begin{array}{l} \mu_M = E(M) \\ \sum_M = \text{cov}(M) = E(M^2) - E(M)^2 \\ \qquad = E(MM^T) - E(M)E(M)^T \end{array} \right\} \quad (9)$$

The advantage of choosing a lognormal *pdf* for *M* is that it enforces the physical constraint that the radiance *M* must be positive. However, normal *pdf*s are easier to manipulate mathematically (e.g., in subtraction operations of RVs) than lognormal *pdf*s, and with proper choice of the population parameters $(\mu_M, \sum_M)$ for normal *pdf*, we can enforce $M > 0$ in the sense that probability *pdf*(*M<0*) is practically zero (due to the fact that the value of *M* is "far" from zero). A more complicated *pdf* (but also more accurate) for *M* can be given with the Johnson distribution family[8], by a fitting procedure that uses the first four moments of *M*. Our choice is to use the simple normal *pdf* for *M* for which the statistics of the detection scores (4) are more easily obtained.

### 5. *Statistics of the detector scores*

The scores, (4), are scalar quantities that embody a spectrally-weighted measure of how similar the measured signal is to the expected target spectrum. The larger the score, the more similar the data resembles the target spectrum. Given the detection scores it is of interest to estimate the probability that a particular score value can be attributed to an $H_0$ scenario or to an $H_1$ scenario.

Using the normal approximation, the signal *M* is distributed by

$$\left\{ \begin{array}{l} M_0 = M \mid H_0 \sim N(\mu_0, \sum_0) \\ M_1 = M \mid H_1 \sim N(\mu_1, \sum_1) \\ \mu_0 = E(M \mid fh = 0); \quad \sum_0 = \text{cov}(M \mid fh = 0) \\ \mu_1 = E(M \mid fh \neq 0); \quad \sum_1 = \text{cov}(M \mid fh \neq 0) \end{array} \right\} \quad (10)$$

where $(\mu_0, \mu_1, \sum_0, \sum_1)$ are computed from the first and second moments of the *pdf*s of the variables (*f*, *h*, $R_0$, $R_t$). The target direction $\delta$ for the matched filter (see (4)) is chosen to be $\delta = \mu_1 - \mu_0$ where we note that $\mu_1$ is a function of the bare surface reflectivity $R_0$, and therefore

$\delta$ is also a function of $R_0$. In practice, $\mu_1$ may not be known a priori, hence, one can use $\alpha$ instead of $\delta$ – a choice that will cause a drop of detection performance that can be estimated with the magnitude of the cosine angle between the vector $\sum_0^{-0.5}\alpha$ and the vector $\sum_0^{-0.5}(\mu_1-\mu_0)$. We note that the drop of performance affects the detection probability in (12) below, which is the 1st stage in the binary integration (to be discussed in section 6) but, can be somewhat mitigated at the 2nd stage of the binary integration where the sum of scores above a given threshold is computed. Equation (4) can be written with (10) as

$$\left\{\begin{array}{l} score=\dfrac{[M-\mu_0]^T\sum_0^{-1}\delta}{\delta^T\sum_0^{-1}\delta} \\ \delta=\mu_1-\mu_0 \end{array}\right\}. \quad (11)$$

If $\sum_0$ is known, and thus is not treated as stochastic, the scores are distributed with normal statistics as two normal distributions with unequal variances located at zero (for $H_0$) and at one (for $H_1$) given by (12)

$$\left\{\begin{array}{l} score\,|\,H_0 \sim N(0,[\delta^T\sum_0^{-1}\delta]^{-1}) = p_0(x) \\ score\,|\,H_1 \sim N(1,[\delta^T\sum_0^{-1}\sum_1\sum_0^{-1}\delta][\delta^T\sum_0^{-1}\delta]^{-2}) = p_1(x) \\ \gamma=\dfrac{E(score\,|\,H_1)-E(score\,|\,H_0)}{\sqrt{Var(score\,|\,H_0)}}=[\delta^T\sum_0^{-1}\delta]^{0.5} \\ P_{false}(\eta)=\int_\eta^\infty p_0(x)dx=2^{-1}[1-erf(\dfrac{\eta}{\sqrt{2(\delta^T\sum_0^{-1}\delta)^{-1}}})] \\ P_{\text{detection}}(\eta)=\int_\eta^\infty p_1(x)dx=2^{-1}[1-erf(\dfrac{\eta-1}{\sqrt{2(\delta^T\sum_0^{-1}\sum_1\sum_0^{-1}\delta)(\delta^T\sum_0^{-1}\delta)^{-2}}})] \end{array}\right\} \quad (12)$$

where $p_0$ and $p_1$ (top two lines of 12) are the *pdf*s for the $H_0$ scores and $H_1$ scores; $\gamma$ is the distance between the means of the scores under $H_1$ and $H_0$ in units of standard deviation of the $H_0$ scores (note that for $\sum_1=\sum_0$, $\gamma = SNR$ of the $H_1$ scores and is a sufficient statistic to completely describe detection performance), we refer to $\gamma$ as "*pseudo SNR*"; the probabilities of detection $P_{\text{detection}}(\eta)$ and false alarm $P_{false}(\eta)$ (bottom two lines) for a given threshold $\eta$ are the cumulative density functions (*cdf*s) of the scores and are given with the error function. The parameter $\gamma$ is related to the separation between $H_0$ and $H_1$ score distributions, but if $\sum_1\neq\sum_0$ $\gamma$ does not completely describe the separation and it is possible for two scenarios with the same $\gamma$ exhibit different performance. If $\sum_0$ is not known *a priori* (e.g., we are asked to predict the scores distributions at a later day for which we do not have $\sum_0$) and thus is a random variable, the statistics of the predicted scores are given by confluent hypergeometric statistics[9] when $\sum_1=\sum_0$; when $\sum_1\neq\sum_0$ the distributions in reference [9] do not apply and must be modified.

## 6. *Combining detector scores and probabilities from multiple scores and areas of regard*

In the general scenario we interrogate the event (a suspicious car) in $J$ areas of regard (see external constraints in (5)) where for the $j^{th}$ area we have $N$ detections scores with probabilities of false alarm and detection under $H_0$ and $H_1$ (given by (11, 12)). Each of the $J$ AOR's can be viewed as a "local detector" that collects $N$ measurements and produces $N$ scores. The challenge is to combine all the $N$ scores for the $J$ regions ( $J \times N$ results) into *one* probability of detection (and false alarm) for the event. For simplicity and ease of notation, we assume an equal number of measurements $N_j = N$ for each of the $J$ areas. We propose to use the radar methodology[3] of "binary integration", also known as "double-threshold detector", and "$m$-out-of-$n$ detector". While detectors that employ binary integration techniques (commonly used in radar) are not optimal in performance, they are easy to implement and are relatively insensitive to a single large interference/clutter that might exist in the scene. No matter what is the energy in the measured signal, the output from the 1st threshold is a binary "1" or "0", and thus binary integration detectors are robust in performance (less susceptible to false alarms) when the background noise/clutter is a non-Gaussian statistics with high tails (reference 3, p293-294) that can produce large scores where one large (false) score may dominate all other scores. With a binary integration method all scores are transformed to "1" or "0" regardless of their numerical value. In our context, the binary integration addresses the problem of deciding if the target is present in the $j^{th}$ AOR given $N$. Then, we address the following question: given the $J$ results what is the probability of detection for the global event (contaminated car).

From a system perspective (the system is a set of $J$ local detectors, each of which produces $N$ measurements) the mathematical statement of the problem is as follows. For the system as a whole the objective is to minimize a given cost function for the global event and to find the parameters (the two thresholds) for each of the $J$ detectors. In order to achieve this objective with the "binary integration" (double-threshold detector) method we need to set two thresholds for each of the $J$ local detectors (we need to set $2 \times J$ thresholds for the system) that together will satisfy the system objective. Let the 1st threshold for the $j^{th}$ local detector be $\eta_{1j}$ and the 2nd threshold be $\eta_{2j}$. We compare the $i^{th}$ measurement (out of $N$ measurements) for a local detector $j$ to the threshold $\eta_{1j}$ and produce a local binary score $s_{ji} = 1$ when $score_{ji} > \eta_{1j}$, or $s_{ji} = 0$ otherwise. We obtain $N$ binary scores for the $j^{th}$ detector. Then, we sum the $N$ binary scores and compare the sum $\sum_{i=1}^{N} s_{ji}$ to the 2nd threshold $\eta_{2j}$, $S_j = \sum_{i=1}^{N} s_{ji} \geq \eta_{2j}$, to produce an integrated detection score $S_j$ that is one when the sum exceeds the threshold value (or zero otherwise) indicating that a target was detected by $j^{th}$ local detector. The value of the 2nd threshold $\eta_{2j}$ is the "$m$" in the name "$m$-out-of-$n$ detector" that is used synonymously with the name "binary integration". The sequence of $N$ binary scores (for a given detector $j$), $s_{ji}$, is a

Bernoulli sequence, and the sum of the scores, $S_j = \sum_{i=1}^{N} s_{ji}$ is a binomial random variable. All the $J$ integrated scores, $S_j$, are fused (with a fusion rule that can take the form of a logical *AND* or *OR* operators, or a majority rule) to produce the system declaration "target is detected". A system with $J$ local detectors is also known as "distributed detectors", "distributed binary integration system", and "distributed detection network". The challenge is to properly set the local detectors' double thresholds.

The solution for combining $J$ local detectors (each with $N$ scores) as a distributed binary integration system (also known as a double-threshold detector, or $m$-out-of-$n$ detector) is given by Han et al.[10] where the cost function for the system (i.e. for the entire car) is chosen to minimize the system probability of a missed detection, $P_{miss\,(system)} = 1 - P_{\text{detect(sys tem)}}$, for a given constraint of constant false alarm (CFAR) system-false-alarm probability, $P_{false\,(system)}$. A specific fusion rule (logical *AND* or *OR*) is chosen to combine all the $J$ scores (each score is produced with a binary integration, double threshold method). The method of solution for the minimization problem is the Lagrange multiplier method. Let's assume that for each of the $J$ local detectors we have $N$ measurements according to (2), $M_{i=1\,to\,N}$ and by assuming a statistical model for the signals (normal statistics in (10)), one can compute $2 \times J$ detection and false alarm probabilities (from (12)) that apply to $score_{ji}$: $P_{\text{d(j)}}(x \geq \eta_{1j}) = \int_{\eta_{1j}}^{\infty} p_1(x)dx$ and $P_{\text{f(j)}}(x \geq \eta_{1j}) = \int_{\eta_{1j}}^{\infty} p_0(x)dx$. With these $2 \times J$ quantitie plus the system false alarm probability, $P_{false\,(system)}$, and $J \times N$ scores (computed from $M_{i=1\,to\,N}$ for the $J$ local detectors) the $J$ 1st threshold $\eta_{1j}$ values and $J$ 2nd threshold $\eta_{2j}$ values are solved for. The solution process involves solving simultaneously $2 \times J$ nonlinear equations. A solution is obtained with numerical optimization routines.

We think of a fusion rule in the form of logical "OR" as the proper choice for detecting a contaminated car that is observed in $J$ AORs because it is unlikely that all the AORs are contaminated (hence we rule out the use of an "AND" operation) and also a majority fusion rule is risky because it is possible that the car will be contaminated only in one AOR. With an "OR" fusion rule we declare a detection if *at least* one (or more) of the $J$ local detectors (operating with the two thresholds binary integration method) produces a detection. Thus, the "OR" fusion rule is more likely to produce better system detection performance.

A full implementation of the Han et al.[10] solution for distributed sensors is not easy (solving $2 \times J$ nonlinear equations), and thus, we give an alternative solution that though is not as optimal is much more practical to use. Our objective, as in Han et al. (1993) is to set the two thresholds $\eta_{1j}$, $\eta_{2j}$ (for each of the $J$ local detectors) such that the global (system) false alarm $P_{false\,(system)}$ is set to be CFAR mode of operation, and to compute the resulting global detection probability $P_{\text{detect}\,(system)}$. We limit ourselves to the "OR" fusion rule. For simplicity, we

also set all the $J$ thresholds, $\eta_{2j}$, such that the false alarm rate for all $j$ are identical. In (13-19) we outline or solution process for a given $P_{false(system)}$. The global false alarm for an OR fusion rule is given by

$$P_{false(system)} = 1 - \prod_{j=1}^{J} (1 - P_{false,j}) \quad (13)$$

where $P_{false,j}$ is the false alarm of the $j^{\text{th}}$ local detector (after applying the second threshold, i.e., at the second stage of the "double-threshold detector" method). In (13) $1 - P_{false,j}$ is the probability of a correct $H_0$ event, and the product $\prod_{j=1}^{J} (1 - P_{false,j})$ is the joint event of all $J$ detectors to get a true (correct) $H_0$ event. False alarm is the complement of the probability of correct $H_0$ event, i.e., $1 - (\text{correct } H_0)$. Each of the false alarm probabilities, $P_{false,j}$, is given by the binomial distribution for the binary integration method as

$$P_{false,j} = \sum_{m=\eta_{2j}}^{N} \frac{N!}{m!(N-m)!} P_{f1j}^{m} (1 - P_{f1j})^{N-m} \quad (14)$$

where $P_{f1j}$ is the false alarm of the $j^{\text{th}}$ detector operating with the 1st threshold (i.e., at the 1st stage of the double-threshold procedure). We note that in (14) $P_{false,j}$ is a function of the 2nd threshold $\eta_{2j}$. The objective is to solve (13, 14) for all $J$ 1st stage $P_{f1j}$ probabilities. For simplicity (and hence lack of optimality in the system performance) we assume in (13) that all $P_{false,j}$ are equal, hence,

$$P_{false,j} = 1 - (1 - P_{false(system)})^{1/J} \quad (15)$$

We substitute (15) in (14) and solve (with a numerical solver) for $P_{f1j}$ as a function of the 2nd threshold $\eta_{2j}$. Due to the large value of $N$ ($N$ can be 100 or more), we may approximate (14) with a Poisson distribution which is a good approximation of a binomial law when $N$ is large and $P_{f1j}$ is small. Because $P_{false,j}$ is a function of both $P_{f1j}$ and $\eta_{2j}$, we need to choose a value for $\eta_{2j}$ in order to solve for $P_{f1j}$. Currently, we pick the value $\eta_{2j}$ that maximizes the detection probability $P_{d(j)}$ for each $j$ (this improves the optimality of our procedure, but still does not guaranty an optimal overall system probability of detection $P_{\text{detect}(system)}$, hence our result is suboptimal with respect to Han et al.). We use (12) to solve $P_{f1j}$ for the 1st threshold $\eta_{1j}$:

$$\left\{ \begin{array}{l} P_{f1j} = \int_{\eta_{1j}}^{\infty} p_0(x)dx = 2^{-1}[1 - erf(\dfrac{\eta_{1j}}{\sqrt{2(\delta_j{}^T \Sigma_{0,j}^{-1} \delta_j)^{-1}}})] \\ \eta_{1j} = erf^{-1}[1 - 2P_{f1j}]\sqrt{2(\delta_j{}^T \Sigma_{0,j}^{-1} \delta_j)^{-1}} \end{array} \right\} \quad (16)$$

where $\sum_{0,j}$ and $\delta_j$ are the covariance (see (10)) and the target signature (see (11)), respectively, for the $j^{th}$ AOR. Given $\eta_{1j}$ we compute the 1st stage local detection probability with (12) as

$$P_{d1j} = \int_{\eta_{1j}}^{\infty} p_1(x)dx = 2^{-1}[1 - erf(\frac{\eta_{1j} - 1}{\sqrt{2(\delta_j{}^T \sum_{0,j}^{-1} \sum_1 \sum_{0,j}^{-1} \delta_j)(\delta_j{}^T \sum_{0,j}^{-1} \delta_j)^{-2}}})]. \quad (17)$$

The second stage local detection probability is given in a similar manner as (14) with the binomial distribution as a function of the 2nd threshold, $\eta_{2j}$, by

$$P_{\det ect,j} = \sum_{m=\eta_{2j}}^{N} \frac{N!}{m!(N-m)!}[P_{d1j}P(H_1)]^m[1 - P_{d1j}P(H_1)]^{N-m} \quad (18)$$

where $P(H_1)$ is the prior probability for $H_1$ event (target present within the *FOV*). When the *FOV* is small compared to the footprints of the contamination (given by the cross-sectional area distribution $\varphi_a(a)$ in section 3.3), $P(H_1)$ is approximately the fraction of the total cross-sectional area within the $j^{th}$ area (*A*/*J* in (5)). Exact values for $P(H_1)$ can be obtained via the simulation for the fill factor $P_f(f)$ discussed in section 3.3 and Appendix A. In general we seek the largest possible threshold that still produces acceptable probability of detection due to the fact that large threshold improves the rejection of exceptionally large clutter (unexpected clutter that is not predicted by the model). With all *J* local detection probabilities, the global (system) probability of detection for an "OR" fusion rule is given in a similar manner as (13) by

$$P_{\text{detect}(system)} = 1 - \prod_{j=1}^{J}(1 - P_{\text{detect},j}) \quad (19)$$

where $1 - P_{\text{detect},j}$ is the probability of a missed detection and the product $\prod_{j=1}^{J}(1 - P_{\text{detect},j})$ is the joint event of all *J* detectors to miss a detection. Detection is the complement of the probability of a miss, hence the system detection probability is $1 - \prod_{j=1}^{J}(1 - P_{\text{detect},j})$. As noted, our solution process is practical for implementation but is not optimal. We can attempt to optimize our choice for $\eta_{2j}$ by repeating (14-19) for different values for $\eta_{2j}$ and chose the value that maximizes $P_{\text{detect}(system)}$.

At present our optimization process for finding the two thresholds $\eta_{1j}$ and $\eta_{2j}$ is as follows. Given $P_{false(system)}$ and *J* in (15) we solve for the false alarm $P_{false,j}$ of the $j^{th}$ local detector. We use $P_{false,j}$ in (14) and find $P_{f1j}$ for a given set-value of $\eta_{2j}$ in (14), say, $\eta_{2j} = 1$. With that $P_{f1j}$ we can compute the 1st threshold $\eta_{1j}$ for the $j^{th}$ local detector in (16), and we also compute the 1st stage detection probability $P_{d1j}$ in (17). We repeat the computation of $P_{d1j}$ for *all* values $\eta_{2j} = 1 \; to \; N$, and choose the specific value $\eta_{2j}$ that maximizes $P_{d1j}$ (this is the best value

for the 2nd threshold). For this "best 2nd threshold" we already know the value of $P_{f1j}$, hence we know the "best 1st threshold" $\eta_{1j}$ given by (16). While not 100% optimal with respect to $P_{\text{detect}(system)}$, due to the constraint of same $P_{false,j}$ for all $j$ in (15), our selection process for the two thresholds works well in our simulations.

## 7. System Requirements

We address the scenario of a contaminated car with fill factor $f$ and contamination thickness $h$ (both $f$ and $h$ are stochastic variables that have fluctuations given by *pdf*s in section 3), subject to the geometry of the problem (see (2)) and the external constraints and sensor parameters (see (5)). The geometry parameters are: the distance of the laser source to the car, $r_{source}$; the distance from the contaminated car (the target) to the detector, $r_{detector}$; and the atmospheric transmission, $t_{atm}$, that is a function of range $(r_{source} + r_{detector})$. Sensor parameters are: total time ($T$) available for scanning a suspected car; sensor acquisition rate, PRF (i.e., measuring $p$ spectral bands every $PRF^{-1}$ seconds); sensor field of view, $FOV$; and the $J$ areas of regard with associated viewed area $A = \sum_{j=1}^{J} A_j$. The average surface density for the contamination $G(g/m^2)$ is given by the product (multiplication) of the contamination intrinsic material density (2.34 g/$cm^3$ for potassium chlorate) and the average thickness of $h$, $E(h)$. This gives the average surface-density of the contamination that is encountered within the $FOV$ under the $H_1$ scenario. The global contamination surface-density within the viewing area $A_j$ is much smaller (the contamination is not spread uniformly over the car's surface) and is given by the product of $G(g/m^2)$ and the prior probability $P(H_1)$. We compute the number of areas of regards $J$, number of samples $N$, and the measurements $M_{i=1 to N}$ (see (2)). The numerical value of $J$ is determined either by subjective requirement such as "need to sample the car at $J$ specific locations", e.g., $J$=5 for: hood, two front doors and trunk area; or by the constraint $J = A/(N \times r_{source}^2 FOV)$, where $N$ is the number of measurements (e.g., number of pixels in a 2D imaging sensor) and $FOV$ is the instantaneous field of view of a pixel. With the solution (section 6) subject to the system's requirements of a given value of CFAR, we obtain the two thresholds, and we use the 1st threshold $\eta_{1j}$ as follows. The numerical value of the two thresholds includes the effect of clutter via the uncertainty that is captured in the statistics of $R_0$. In most detection scenarios clutter noise is much larger than the sensor noise (noise-equivalent spectral radiance, NESR), we expect that state of the art sensors (NESR ~$10^{-8}$ $W/cm^2/sr/cm^{-1}$) is sufficient. A system design involves a tradeoff between many parameters (data acquisition parameters and scenario parameters). Our stochastic model for contaminated surfaces can help in studying these tradeoffs. For example, given a requirement of CFAR operation we can use our model to compute detection thresholds $(\eta_{1j}, \eta_{2j})$ as a function of the contamination amount ($h$) and to tie the numerical value of the thresholds to the system's

characteristic noise. In addition, with our stochastic model we can study the effect of stochastic fluctuations in various parameters ($h$, f, $R_0$) on the detection performance, as well as studying the interaction between the external system parameters ($T$, $PRF$, $FOV$) and the detection performance.

We view the utility of our stochastic model for rough surface contamination in two types of scenarios with regard to the evaluation and the design of a detection system. In the first scenario we evaluate the performance of a given sensor in a detection scenario where the contamination parameters are unknown. Thus, in this scenario the external constraints (5) are given (i.e., a sensor with $FOV$, and $PRF$) and the contamination variable ($h, f, R_0$) in (2) are variables. Please note that in (5) the detection is only based on the total number of measurements $J \times N$ (where each of the $N$ measurements contain $p$ spectral bands) and that $N$ can be achieved by measuring the $j^{\text{th}}$ AOR with an imaging system that collects $N$ pixels, or a sensor with a single pixel that collect $N$ measurements. Thus, if the $FOV$ of a system and the range to the suspected car is such that for a given $j$ (e.g., $j$=1 is the front door and the sensor is at a distance $r$ from the car) is such that the illuminated footprint $FOV \times r^2$ on the car is equals to the door's area, then $N$ can be achieved by sequential measurements. On the other hand, if the $FOV$ is such that there are $N$ pixels within the door's area, then with an imaging system "one" measurement can provide the $N$ samples in (2, 5). We remind the reader that the fill factor is a function of the sensor's FOV as well as a function of the contamination cross-sectional foot-print and the contamination level. With our model we can estimate the sensor detection probability as a function of the contamination level. The sensor intrinsic external constraints ($FOV$, $PRF$) together with the constraints about the detection scenario ($T$, $A$, $J$) are assumed to be given. With our model we can estimate the detection probability $P_{\text{detect}}(h, f, R_0 \mid CFAR, FOV, PRF, T, A, J)$ as a function of the contamination thickness ($h$), the fill factor ($f$) and the rough surface reflectivity ($R_0$), for a given false alarm (CFAR) and the external constraints ($FOV$, $PRF$, $T$, $A$, $J$). The second scenario for the utility of the model is to answer the following question: "What should be the best sensor parameters ($FOV$, $T$, $PRF$, $A$) for given a contamination scenario with ($h, f, R_0$)?" For this utility scenario we can compute the detection probability $P_{\text{detect}}(FOV, PRF, T, A, J \mid h, f, R_0)$. Setting a value for CFAR depends on operational considerations. For example, if the scenario is of a car-stop checkpoint where a car is inspected with a sensor and when an initial detection is declared, the car is diverted for a further (more thorough) check. If the team at secondary checkpoint can handle a load capacity of checking one car out of 20 (5%), then the CFAR for the initial checkpoint (14-19) can be set to $CFAR$=0.05. The larger the CFAR is, the higher the detection probability is, and thus the probability of missing the presence of a contaminated car is reduced (which is the primary goal of the checkpoint).

There are three key parameters that most effect the overall detection: the number of measurements ($N$), the prior probability $P(H_1)$ of viewing a contaminated area, and the *pseudo SNR* parameter $\gamma$ (given in (12)) which is related to the strength of the $H_1$ scores (i.e., $\gamma$ increases with increased target signal and is inversely proportional to the variance of the rough

surface $\Sigma_0$). The lower $P(H_1)$ is, the larger $N$ should be in order to enhance the likelihood of intercepting the contamination present in $A$ with some of the laser shots. The larger $\gamma$ is, the higher the detection probability is. We explore the interaction between the different variables in section 8.

## 8. Results

We explore the parameter space ($h, f, R_0, N, J, P(H_1)$) with regard to probability of detection, presented in section 8.1, and also present a case studies giving the system detection performance for detecting specific contaminated cars (section 8.2). In all our simulations a zero-mean additive Gaussian noise with standard deviation of 0.005 was added to the simulated measurements in (2). The objective system false alarm was set in all simulations to be CFAR=0.05. The geometry for the simulations assumes backscattering angle $\theta = \theta_i$ in (1), and $K_{system}$=1 in (2). We note that most of the fluctuations in the simulated measurements are due to the stochastic nature of the RVs. Additive noise is usually easy to handled in detection algorithms because it is white (spectrally isotopic). The challange in detection algorithm is how to handle "structured" noise in the form of clutter, which is given in our work by the *pdf* of $R_0$. Our contamination is a potassium chlorate material (specific density of 2.34 g/$cm^3$). In all simulations $g\Delta n$ in (1) is set to zero for simplicity, the contamination is potassium chlorate, and the extinction coefficient $\alpha$ was taken from the KBr pellet measurements in reference 1. Note that the RV $f$ (fill factor) is conditioned to the $H_1$ event, i.e., it is the fraction of contaminated area within the illuminated spot (we assume that the *FOV* matches the laser's beam divergence) when contamination is actually present. The prior probability for $H_1$ event is (roughly) the portion of the *measured* area that is contaminated, where the measured area includes subareas that are not contaminated. The parameter space is > 3 and thus it is not possible to simultaneously display the intricate interaction between the variables (for this we need a "7D plot"—6 independent parameters plus a probability of detection as a dependent variable). We remind the reader that with the external constraints in (5), one can relate physical parameters of the sensor (FOV, PRF, and distance to the surface), and acquisition parameters (total area, $A$, to sample and time, $T$, to acquire the measurements) with the detection parameters ($N$ and $J$). For example, given $N$=100 and $J$=4, e.g., for two doors ($j$=1, 2), hood and trunk ($j$=3, 4); or $j$=1, 2 for painted/unpainted vertical surfaces, and $j$=3, 4 for painted/unpainted horizontal) and a sensor with 1$mr$ linear field of view (solid angle FOV is $10^{-6}$ sr) at a distance of 20 $m$ (i.e., 2 $cm$ illuminated spot) and PRF of 10Hz, implies that total time for measuring the contaminated car is $T = 40s = J \times N / PRF$, and the total car's area that is measured is $A = 1600\,cm^2 = N \times r^2 FOV \times J$ (i.e., a small 10$cm$ by 10$cm$ area for each of the 4 $J$'s).

*8.1 Exploring the parameter space*

We explore the parameter space ($R_0$, $h$, $f$) as is used in our 2nd order statistics (mean and variance in equations 9-12) and its effect on detection. We compute (13-19) the double thresholds, the overall global (system) detection $P_{\text{detection}}(\text{c}ar)$. We present a few 3D plots to show the complex interaction between the key parameters that govern the detection scenario: $(P_{\text{detect(system)}}, \gamma, P(H_1), N)$. We constrain the desired overall (global) system CFAR to be $P_{\text{false-alarm}}(\text{c}ar) = 0.05$. To explore the parameter space we selected different combinations of mean values for $f$ and $h$, E($f$) and E($h$), respectively, and arbitrarily set the variances as follows: the standard deviation of $h$ is 10% of its mean value; the standard deviation (*std*) of $f$ is the *minimum* value between $E(f)/5$ and $[1-E(f)]/5$ (where the value 5 is 5-standard deviations) to ensure that for normally distributed $f$, the constraint $0 < f \le 1$ is met. Our choice for standard deviation of $f$ enforces a low standard deviation near the endpoints ($f$=0 and $f$=1) and a high standard deviation in the middle ($f$=0.5). Our choice for *std* can be interpreted as follows: a low *std* near $f$=0 may occur for a sensor with large *FOV* viewing sparse contamination with a small cross-sectional area; a small *std* at $f$=1 may occur for a sensor with a small *FOV* and contamination with large cross-sectional area; and for $f$~0.5 the sensor *FOV* matches the *size* of the contamination footprint and how the *FOV* and contamination overlap (intersect) can produce both large and small values of $f$, hence a large *std*. The mean of $R_0$ is taken from for lab measurements[1] of rough aluminum where $a_0 = 6.96 \times 10^{-8} cm^2$, $b_0 = -6.98 \times 10^{-4} cm$, $c_0 = 0.25$ and the corresponding standard deviations were arbitrarily set at $(1 \times 10^{-7} cm^2, 1 \times 10^{-5} cm, 1 \times 10^{-3})$ as we do not have enough lab data to estimate standard deviations. Upon availability of data we can update the standard deviation values. The Fresnel coefficient $\rho_0$ is for pure aluminum (whose reflectivity across the LWIR is ~0.99). Due to the large aluminum reference the effect of surface reflection from the target was small and allowed us to set $a_t = b_t = c_t = -\infty$ in (1). The 19 ($p$) wavenumbers in our simulations correspond to available $CO_2$ laser wavelengths (9-11$\mu m$), given in $cm^{-1}$ as 934.93, 942.42, 949.49, 956.21, 969.18, 974.66, 975.9, 978.47, 982.13, 986.58, 1031.5, 1039.4, 1046.9, 1052.2, 1057.3, 1070.4, 1074.7, 1078.6 1083.4.

In Fig. 1a we show the interaction between $(P_{\text{detect(system)}}, \gamma, P(H_1), N)$ for a given CFAR=0.05 and for one region ($J$=1) of aluminum rough surface. For each combination of E($f$) and E($h$) the pseudo-SNR parameter $\gamma$ was computed, and a series of system detection probabilities were computed for different values of $N$ and P($H_1$). The figure shows that the overall system detection probability increases as $P(H_1)$, $N$, and $\gamma$ increase. In Fig. 1b we show the relationship between $\gamma$ and the means of the fill factor $f$ and the contamination thickness $h$ (may be converted to surface contamination density via $G(\mu g / cm^2) = 234 \times E(h)$ where $h$ is in microns). The figure shows the monotonic increase of $\gamma$ with $h$ and $f$.

We can also use the stochastic model to set sensor requirements for a contamination scenario. In Figs. 2a and 2b we show an expanded portion of Fig 1. Note that Fig. 2a, for

example, can be used to determine what values for parameters $N$, $P(H_1)$, and $\gamma$ are required to achieve a particular system-level probability of detection. For example, assuming a desired $P_{\text{detect(system)}} \geq 0.8$, any point lying on or above the red contour surface will satisfy the desired condition (given the *pdf* choices used to create the figure). The mapping is not unique (many sets of values for $N$, $P(H_1)$ and $\gamma$ will satisfy the condition) and therefore it is difficult to invert Eqs. (13-19) to solve for $N$, $P(H_1)$ and $\gamma$ given $P_{\text{detect(system)}}$. However, desired information about $N$, $P(H_1)$, and $\gamma$ given $P_{\text{detect(system)}}$ can be read off of plots such as Fig. 2a. The parameters $N$, $P(H_1)$, and $\gamma$ all relate to sensor requirements (external constraints in Eq. (5))—$N$ relates to the time to detect and *FOV* of the sensor, $P(H_1)$ depends on the *FOV* and the nature of the contamination, and $\gamma$ depends both on the nature of the contamination (thickness $h$, fill factor $f$, surface density G) and the sensitivity of the sensor (laser power, noise level, etc.).

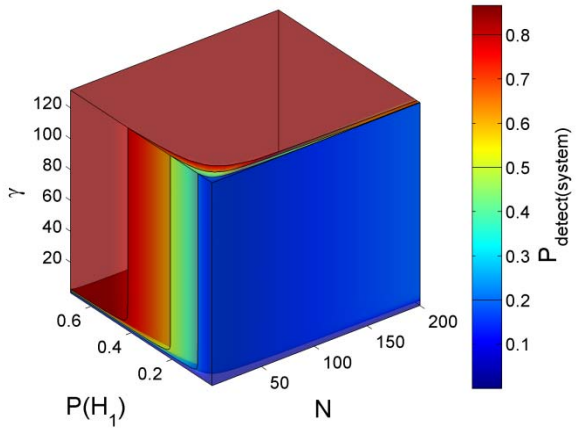


**Fig. 1a** System detection probability for one area of regard ($J$=1) of rough aluminum as a function of number of measurements ($N$), prior probability $P(H_1)$, and the pseudo *SNR* parameter $\gamma$. Contour surfaces show where $P_{\text{detect(system)}}$ = constant. Three contour surfaces are shown at $P_{\text{detect(system)}}$ values of 0.2 (blue), 0.5 (green/yellow), and 0.8 (red).

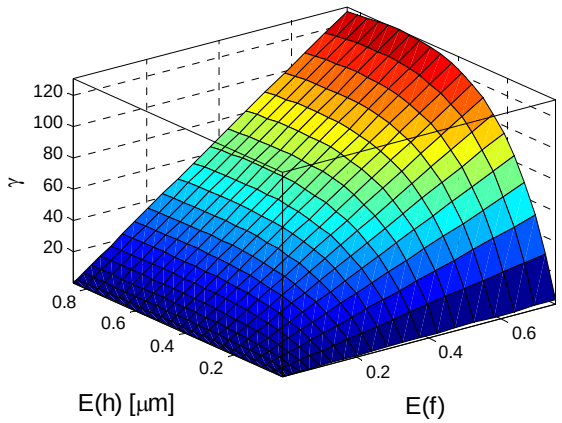


**Fig. 1b** Pseudo-*SNR* parameter $\gamma$ as a function of the mean fill factor, $E(f)$, and the mean contamination thickness, $E(h)$, where the surface contamination density is $G(\mu g / cm^2) = 234 \times h$ where $h$ is in microns).

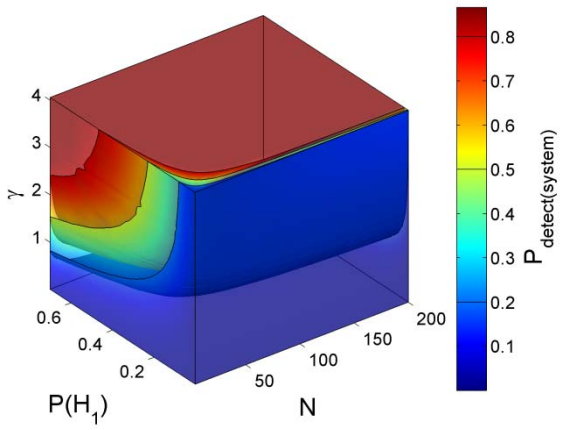


**Fig. 2a** An expanded view of Fig. 1a to show the behavior for $\gamma$<4.

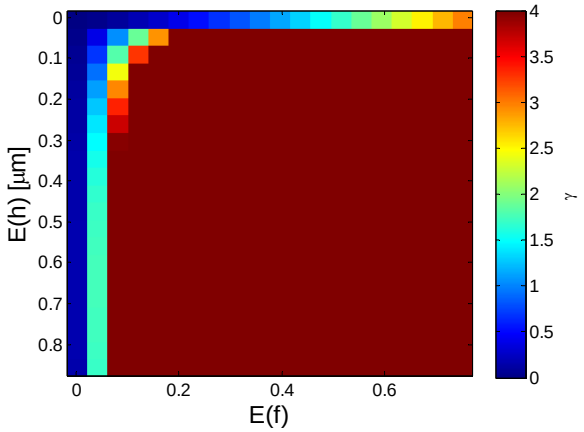


**Fig. 2b** An expanded view of Fig. 1b to show details of pseudo *SNR* parameter $\gamma$ as a function of fill factor and contamination thickness. Combinations of E(*h*) and E(*f*) resulting in $\gamma$>4 are shown as dark red pixels, $\gamma$<4 are mapped to other colors as shown.

In Fig. 3 we show the improved detection when 3 rough aluminum AOR (*J*=3) are used for detection (19) instead of only one AOR. The improved detection can be observed by comparing Fig 3 with Fig. 2a where it is evident that the contours for high detection probability (brown and red colors) in Fig. 3 spread to the direction of lower values of $N$, $P(H_1)$, and $\gamma$.

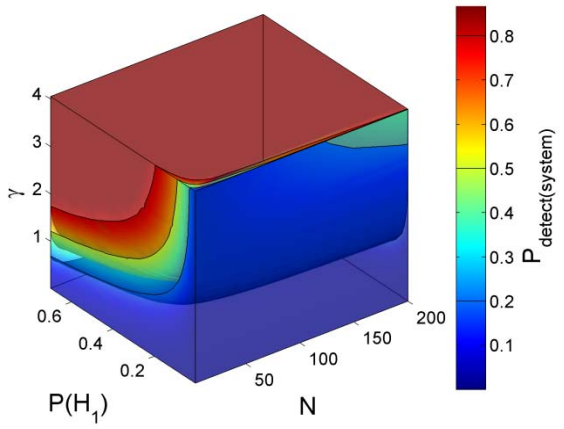


**Fig. 3** Same as Fig. 1a but *J*=3 areas of regard are used for detection in (19).

We explore the effect of a different rough surface material, painted aluminum, which may be more realistic for a car. We set $a_0 = -3.47\times10^{-7}\,cm^2$, $b_0 = -4.78\times10^{-4}\,cm$ , $c_0 = 1.07$ (derived from lab measurements[1]) and the corresponding standard deviations are the same as those previously selected for rough aluminum $(1\times10^{-7}\,cm^2, 1\times10^{-5}\,cm, 1\times10^{-3})$. Due to the low reflectivity of the painted aluminum ( $\rho_0 \sim 0.07$ across the 19 laser wavelengths), the potassium chlorate rough-surface parameters (see equation 1) were used and set to $a_t = -3.20\times10^{-7}\,cm^2$, $b_t = 2.07\times10^{-3}\,cm$ , $c_t = -2.58$ (derived from a lab measurements[1]). Corresponding standard deviations were set arbitrarily to $(5\times10^{-9}\,cm^2, 5\times10^{-5}\,cm, 5\times10^{-3})$, as we do not have enough lab data to estimate standard deviations.

We observed that the painted aluminum surface produced less signal (*M* in equation 1) and that the pseudo SNR parameter $\gamma$ was about factor 3 reduced from the rough aluminum surface (in Fig. 1b). Thus, the system detection probability will be reduced given the same *E*(*h*) and *E*(*f*) values. One may use Figs 1a (or 2a) to obtain a value of interest for $\gamma$ that produce the desired system detection probability, and find in Fig. 1b (or 2b) the values for *E*(*h*) and *E*(*f*) that corresponds to a value of $3\gamma$. These values of *E*(*h*) and *E*(*f*) are the one that corresponds to contaminated painted aluminum surface.

*8.2. A case study: the detection of a contaminated car*

We explore the detection scenario with two case studies (simulation 1 in Figs. 4-6, and simulation 2 in Figs 6-7) for a contaminated car at a distance of 20*m* to be detected in 10s where two areas of regard (*J*=2) are sampled: the first AOR is rough aluminum, and the 2nd AOR is a painted rough aluminum (the same parameters for $a_0$, $b_0$, $c_0$ presented in Section 8.1 were used here). The *pdf* for *h* is a ramp (consistent with our expectation that a high target transmission is more likely than a low transmission) and thus, $P_h(h) = 2\dfrac{h_{\max} - h}{(h_{\max} - h_{\min})^2}$ for $h_{\max} = 0.75\mu m$ and

$h_{\min} = 0.01\mu m$ (Section 3.2). For this distribution $E(h) = 0.25\mu m$. For the *pdf* for *f* we present two case studies. First case is computed (Appendix A) from cross-sectional area (footprint or spill distribution), $\varphi_a$, measured by MIT-LL (large majority of the footprints are small for which the key parameter $P(H_1)$ is large—about 0.4—see *pdf* of fill factor and $P(H_1)$ in Fig A1). For case 2 we simulate the contamination footprint (Fig. A2) such that large footprint are more likely in $\varphi_a$ for which the key parameter $P(H_1)$ is small (0.07). In our scenario the laser linear FOV (and beam divergence) is 1*mr* (i.e., a 2*cm* spot size on the car) and the laser is configured in the traditional backscatter lidar configuration. The system constant $K_{system} = L_{source}(\theta_i)\frac{t_{atm}}{(r_{source} + r_{\text{detector}})^2}$ is set to be one in (2). The laser system operates at 10 *Hz* and acquires *N*=50 spectral measurements for each of the AORs (each of the *N* measurements contains 19 wavelengths in the LWIR range). The total acquisition time for *J*=2 is $T = 10s = J \times N / PRF$ as required.

In Fig. 4 we show results for case 1 for the effect of the second binary threshold $\eta_{2j}$ (given in equation 18) for the two local detectors (*j*=1 and *j*=2) on the local detection probability $P_{\text{detect},j}$ and also on the system-level detection probability $P_{\text{detect(system)}}$ (see (19)). The pseudo-*SNR* parameter γ equals 2.7 and 1.2 for *j*=1 and *j*=2, respectively, meaning that it is an easier detection problem to detect potassium chlorate signals on rough aluminum rather than painted aluminum. As a result, the *j*=1 region shows better performance than *j*=2 (maximum value of $P_{\text{detect},j=2} = 0.926$ whereas $P_{\text{detect},j=1}$ exceeds this value for $\eta_{21} < 8$). The system-level performance shows a larger probability of detection at the same value of $\eta_{2j}$, or alternatively for the same probability of detection a larger threshold may be used. We desire the largest possible threshold that still produces high probability of detection because high threshold improves the rejection of exceptionally large clutter (unexpected clutter that is not predicted by the model).

In Fig. 5 we show the overall system detection probability $P_{\text{detect(system)}}$ in (19) for case 1 as a function of all possible combination of thresholds $\eta_{2j}$ (given in 18). The asymmetry in Fig. 5 is interesting. It shows that it is more important to optimize $\eta_{21}$: given an optimal value of $\eta_{21}$, it is less important ($P_{\text{detect(system)}}$ is less sensitive) to the value of $\eta_{22}$. This makes sense since *j*=1 is a better region (higher performance) than *j*=2.

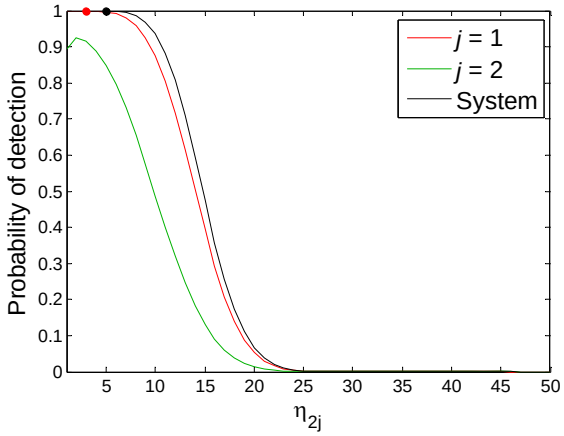


**Fig. 4** Detection probability of local detectors $P_{\text{detect},j}$ in (19) for simulation 1 (footprint contamination Fig. A1) as a function of the 2nd binary threshold $\eta_{2j}$. $j$=1 is AOR for rough aluminum, and $j$=2 is AOR for painted aluminum surface. $P(H_1)$=0.4. The system detection probability, under the condition that $\eta_{21} = \eta_{22}$, is also shown in black. $P_{\text{detect},j=2}$ reaches a maximum of 0.926 at $\eta_{22} = 2$. Red dot shows the largest $\eta_{21}$ such that $P_{\text{detect},j=1}$ exceeds a detection probability of 0.999 (occurs at $\eta_{21} = 3$). Black dot shows the location where the system detection probability exceeds 0.999 (occurs at $\eta_{21} = \eta_{22} = 5$). Combining the two regions allows larger $\eta_{2j}$ thresholds to achieve the same detection probability and will result in more robust performance.

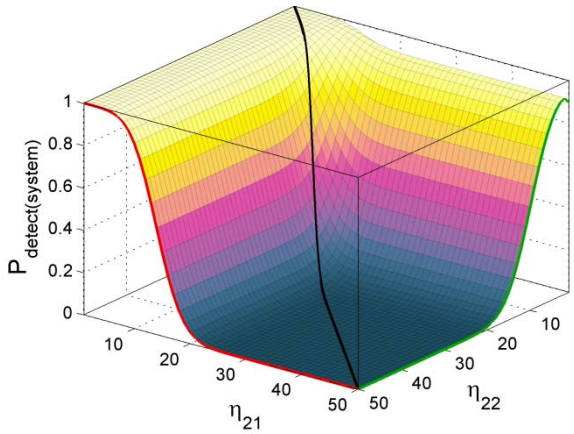


**Fig. 5** Overall system detection probability $P_{\text{detect(system)}}$ in (19) for case 1, as a function of all possible combinations of 2nd thresholds $\eta_{2j}$ in (18). $P(H_1)$=0.4. $\eta_{21}$ is 2nd threshold for $j$=1 (rough aluminum) and $\eta_{22}$ is 2nd threshold for $j$=2 (painted aluminum). Black line occurring along the diagonal (where $\eta_{21} = \eta_{22}$) is the same black line appearing in Fig. 6; red and green lines appearing at $\eta_{22} = N$ and $\eta_{21} = N$, respectively, are the same as in Fig. 4 (at $\eta_{2j} = N$ the detector will never alarm and thus information from the $j^{\text{th}}$ region is discarded). Maximum of $P_{\text{detect(system)}}$ occurs at $\eta_{21} = 1$, $\eta_{22} = 2$ at a value of 0.9999996.

In Figs 6-7 we present the detection for case 2 (Fig. A2, with low $P(H_1)$=0.07). The combination of thresholds ($j$=1 and $j$=2) is advantageous to produce a higher overall system detection probability compared to the individual regions. Fig. 6 in comparison to Fig. 4 shows the importance of the $P(H_1)$ parameter, where in spite of the large pseudo-*SNR* parameter γ (equals 16.9 and 7.1 for $j$=1 and $j$=2, respectively) that is much larger than the γ's in Fig. 4, the overall system performance is worse than in Fig. 4 because $P(H_1)$ was reduced from 0.4 in Fig. 4 to 0.07 in Fig. 6. The reduction in $P(H_1)$ means that the contamination is more sparse and target material is less frequently encountered by the sensor. The parameter $P(H_1)$ plays a crucial role in system performance (i.e., detection probability) as is demonstrated in Figs. 1-3. The large effect of $P(H_1)$ can also be seen in the performance of the two individual local detectors ($j$=1 for rough aluminum and $j$=2 for painted aluminum). In Fig. 4 a difference of 1.5 units in γ (2.7 − 1.2) between the two local detectors (red and green lines), results in large difference in detection probability (for the same threshold), while a difference of 9.8 units in γ (16.9 − 7.1) in Fig. 6 makes very little difference in detection probability (the red and green lines are almost identical).

Note that in the second simulation the best performance is clearly given by $\eta_{21} = \eta_{22} = 1$, i.e., the presence of a single non-zero value $s_{ji}$ for $i = 1,2,...,N$ and a given $j$ is enough to declare that the $j^{th}$ region is contaminated. This does not mean that the remaining $N-1$ zero-valued scores were "wasted" and that one could have set $N = 1$ and achieved the same performance. Because of the low probability of $P(H_1)$, a large $N$ is required in order to increase the likelihood that the contamination is viewed in at least one of the $N$ measurements.

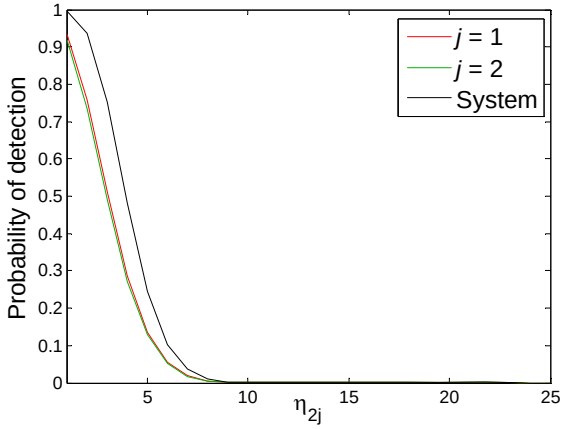


**Fig. 6** Same as Fig 4 but for contamination footprint (case 2) of Fig. A2. $P(H_1)$=0.07. Individual detection probability $P_{\text{detect},j}$ attain a maximum of 0.934 and 0.919 for j=1 and j=2 respectively at $\eta_{2j} = 1$. Maximum detection probability for the system is 0.995 at $\eta_{2j} = 1$.

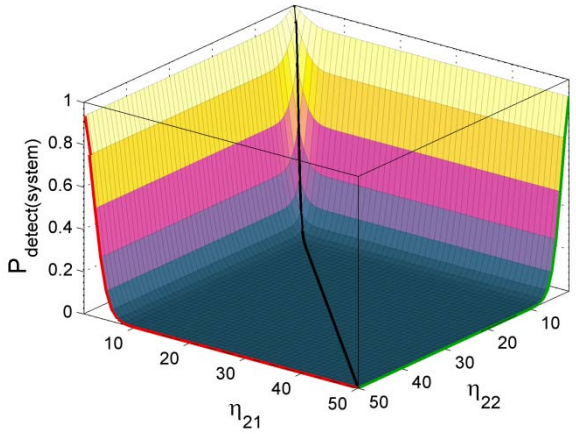


**Fig. 7** Same as Fig. 5 but for contamination footprint (case 2) of Fig. A2. $P(H_1)$=0.07.

## 9. Summary

We developed a framework to evaluate the performance of a system whose objective is the detection of a contaminated car. Our approach is a "system approach" where external constraints (5), such as time to detect, area to scan, distance to the car are input parameters. Our algorithm employs a data fusion approach known as a distributed binary integration system (also known as a double-threshold detector, or *m*-out-of-*n* detector) in order to combine the individual detection results from multiple scans over several potentially contaminated areas. Our system consists of *J* areas of regard (e.g., hood, doors, etc) that are scanned with an active laser source (*p* wavelengths). Our detection algorithm utilizes the matched filter concept (which is optimal for additive Gaussian noise; in our detection scenario the clutter noise is not additive) together with Neyman-Pearson methodology of *CFAR* operation mode. We view our system as a "distributed binary integration system", a methodology that is used in radar literature. Each of the *J* areas is viewed as a "local detector" and the system fuse the local detectors output (fusing rules can be logical AND, OR, or majority rule; we chose the OR logic in this report in order not to miss a detection) into a "global" detector (i.e., "the system") that produces a declaration "target is detected". We operate each of the detectors with the "binary integration, double threshold" radar methodology, a methodology that is robust to strong clutter fluctuations. From each of *J* areas we obtain *N* spectral measurements (each measurement contains *p* spectral bands). For a given constraint of false alarm (*CFAR* mode of operation) we produce the desired operational thresholds for each of the *J* local detectors. Our solution is not optimal with respect to overall detection (or missed detection) but it is much simpler for implementation than the optimal solution given by Han et al.[10] where he minimizes the probability of a missed detection for a given CFAR. In our detection scenario the car is viewed as a rough surface that is partly contaminated with a given amount of contamination. In our detection model all the scenario parameters (contamination thickness *h*, fill factor *f,* and the car's reflectivity $R_0$) are random variables with probability functions.

We think that building a detection system will require the "snapshot advantage architecture" that enables the acquisition on $J \times N \times p$ measurements within a time $T$ (traditional pushbroom/whiskbroom types of acquisitions are much less efficient and produce lower signal-to-noise ratios). The framework that we developed in this report will be the basis for developing a system approach for a Raman detection system and for a passive infrared system where the incidence on the contaminated car is the ambient thermal radiation. A system design involves a tradeoff between many parameters (data acquisition parameters and scenario parameters). The stochastic model for contaminated rough surface with external system parameters is a useful model for designing and prediction the performance of a detection system. Given a requirement of *CFAR* operation we are able with our model to compute detection thresholds $(\eta_{1j}, \eta_{2j})$ as a function of the contamination amount (*h, G*). In addition, with the model we can study the effect of stochastic fluctuations in various parameters ($h, f, R_0$) on the detection performance, as well as studying the interaction between the external system acquisition parameters (*T*, *PRF*, *FOV*) and the detection performance.

With our stochastic model we can explore the probability of detection for a given sensor (e.g., specific *FOV*, *PRF*) under variable contamination scenario (e.g., $h, f$), $P_{\text{detect}}(\text{contamination} \mid sensor)$, and the probability of detection for a given contamination scenario for a sensor with variable properties (e.g., *FOV*, *PRF, T*). We can also use the stochastic model to set sensor requirements for a contamination scenario. For example, Fig. 2a can be used to determine what values for parameters $N$, $P(H_1)$, and $\gamma$ are required to achieve a particular system-level probability of detection, say, $P_{\text{detect(system)}} \geq 0.8$. The parameters $N$, $P(H_1)$, and $\gamma$ all relate to sensor requirements (external constraints in Eq. (5)) — $N$ relates to the time to detect and *FOV* of the sensor, $P(H_1)$ depends on the *FOV* and the nature of the contamination, and $\gamma$ depends both on the nature of the contamination (thickness *h,* fill factor *f,* surface density G ) and the sensitivity of the sensor (laser power, noise level, etc.).

In the report we showed an example of exploring the parameter space ($h, f, R_0, N, J,$ $P(H_1)$ with regard to probability of detection, and we also explored the *pdf* space for the different variables and recommended what *pdf*s to use for each variable for physical simulations. The most important parameters that affect the overall detection probability are the number of measurements ($N$), the prior probability of $P(H_1)$ of the contaminated areas, and the *pseudo-SNR* parameter $\gamma$ which is related to the strength of the $H_1$ scores. The lower $P(H_1)$ is, the larger $N$ should be in order to enhance the likelihood of intercepting the contamination present in $A$ with some of the laser shots. The larger $\gamma$ is, the higher the detection probability is. With our probability model we can explore the parameter space and study the tradeoffs between parameters that affect the overall system detection. We presented 3D plots (section 8) that demonstrate the interaction between parameters and an example for the detection of a contaminated car with a $CO_2$ tunable laser (19 wavelengths) system. In our examples a clutter distribution for $R_0$ was assumed. Our choice may not accurately represent the variability of the clutter observed in practice. Thus, a key recommendation is to better characterize both the clutter

and target variability (for example, through empirical measurements) so that our performance estimates may be updated.

This report is the foundation (framework) on which we will develop a stochastic detection model for passive infrared remote sensing system and for active Raman detection system. In the next report we plan to do the following:

- For Raman detection $R(\theta,\theta_i)$ in (1) will be modified to comply with the physics of Raman scattering.
- For passive remote sensing (2) will be replaced by Eq. (11) of [1].
- We will complete our theory for the probability of a fill factor based on the random distribution of centers in a hyper volume, and the geometry of intersection between the *FOV* shape (rectangular, circle, and ellipse for tilted surfaces) and the contamination footprint-shape.
- We will explore the effect on overall system performance (19) by using a target direction $\delta \to \alpha$ instead of $\delta \to \mu_1 - \mu_0$ in (11).
- We will optimize our solution for maximizing system performance by allowing each of the local detectors in (15) to have separate probability of false alarm.
- We will explore the quality of using 2nd order statistics (mean and variance) in (12) with histogram computed from sampling the RVs.
- We will explore the probability space of the RVs (i.e., the parameters that control the shape of the *pdf*s in section 3) and its effect on system detection probability.

## Appendix A. Fill factor probability

We estimate the fill factor of the contaminated by a brute force approach where we simulate the random contamination on the surface as produced by a given size distribution $\varphi_a(a)$ of the contamination events. Within each spot the material thickness ($h$ in equation 1) is not necessarily uniform, but the mean surface density of the material is given by $G$=2.34×E($h$), where 2.34 $g/cm^3$ is the intrinsic density for potassium chlorate $E(h)$ is the average height of the contamination (i.e., $G$ is the average contamination surface computed over all of the "spots" in Figs. A1 and A2). The sparsity of the contamination "spots" in Figs. A1 and A2 is given by the parameter $P(H_1)$ in (18) is a key parameter that affect system performance (see section 8). Accurate computation of $P(H_1)$ is affected by the size of the sensor's *FOV*, because sparsity is "measured" with regard to *FOV* (details, below). Figs. A1and A2 are used in section 8.2 as case studies for contaminated areas of a car. The general idea behind the simulations is that we assume that the locations of the target particles (their centers) are uniformly distributed on the surface[7]. Then, we randomly placed a square field of view with area $A_{\mathrm{FOV}}$ ($m^2$) on the simulated contaminated surface and count the area $\mathrm{A_t}$ ($m^2$) for the target (contamination) within the field of view. The ratio $\mathrm{A_t}/A_{\mathrm{FOV}}$ is the fill factor.

Details of the simulation are as follows. Let $a$ denote the cross-sectional area of a single contamination event (i.e., a fingerprint, a single particle, a thin film, or a spill of many particles). We make the following assumptions: a surface of with total area, $A$, is potentially contaminated with multiple contamination events. The contaminated area of all target events is $A_t$, meaning that the prior probability of contamination is $A_t/A$; the likelihood that any infinitesimal portion of the total area is covered by contamination is uniform; the likelihood that a single contamination event is of a certain cross-sectional area is given by *pdf* $P_a(a)$ (computed from $\varphi_a(a)$ in section 3.3), contamination events are assumed to be circular. Areas from multiple contamination events may not overlap (reasonable for sparse contamination).

Under these conditions, a simulated surface is populated in a multi-step process. The simulated surface is a digital image where each pixel in the image is of area $A_{pixel}$ .The digital image is initialized with each pixel taking a value of zero. At the end of the generating process, the digital image will contain a value of the area within each pixel that is covered by contamination. The simulation steps are as follows:

1. Determine average number of contamination events needed to achieve $A_t$: $N_t = \mathrm{E}(a)/A_t$ where $\mathrm{E}(a)$ denotes the average contamination event area (expected value).
2. Sample $N_t$ contamination target events from *pdf* $P_a(a)$ to obtain $a_i$, $i$=1,2,…,$N_t$. For convenience, sort the contamination events in order of descending area.
3. Place the $i^{\text{th}}$ contamination event by choosing a pixel at random which will serve as the center of the contamination event, excluding pixels that would cause overlap between contamination events. For the first contamination event, no pixels are excluded. Note that contamination events smaller than a single pixel may be placed into an already contaminated pixel if the area of contamination in that pixel is $1- a_i/A_{pixel}$ or less, though this will happen with a reduced probability.
4. If $a_i > ¼\pi A_{pixel}$ the contamination event must span multiple pixels (the fraction $\pi/4$ accounts for the difference in linear dimension between a circular contamination and a square pixel), and the event is placed in the image using a Euclidean distance transform: all pixels within a distance of $r_i$ units will be assigned an area of $A_{pixel}$, where $r_i$ is the corresponding radius in pixels of the contamination event if it were circular. Note that this step is an approximation, since edge pixels around the contamination would more accurately be represented with values less than $A_{pixel}$.
5. If $a_i \leq ¼\pi A_{pixel}$ the contamination event can be contained entirely within a single pixel, and a value of $a_i/A_{pixel}$ is added to the current value of the pixel. This additive adjustment is the increase the contaminated area within the pixel due to the additional contamination. Note that this step ignores the fact that a contamination event may not necessarily occur in the exact center of a pixel and could still span over multiple pixels.
6. Once all contamination events are placed in the image, the sensor *FOV* is translated across the image computing the total contaminated area within the *FOV* at each *FOV* location; the fill factor $f$ as seen by a sensor is obtained by dividing by $A_{\mathrm{FOV}}$.

A histogram of $f$ gives an estimate of $P_f(f)$ as seen by a sensor; i.e., it gives the probabilities for the sensor to observe a specific value of $f$. In addition the simulation can give $P(H_1)$ given by the ratio of number of *FOV*s that *are not* empty (i.e., *FOV*s that contain any target material) to the number of *FOV*s ($A/A_{FOV}$) that are contained in the area $A$. For a "small" *FOV* (e.g., an *FOV* that is smaller than the size of the contamination "spots" in Figs A1 and A2), $P(H_1)$ is simply given by the fraction of the area occupied by the target material, $A_t/A$. Hence, $P(H_1)$ can be viewed as a global (macro) property of the contaminated surface, and $G$ is the local (micro) property of the contamination surface density of the contamination events ("spots").

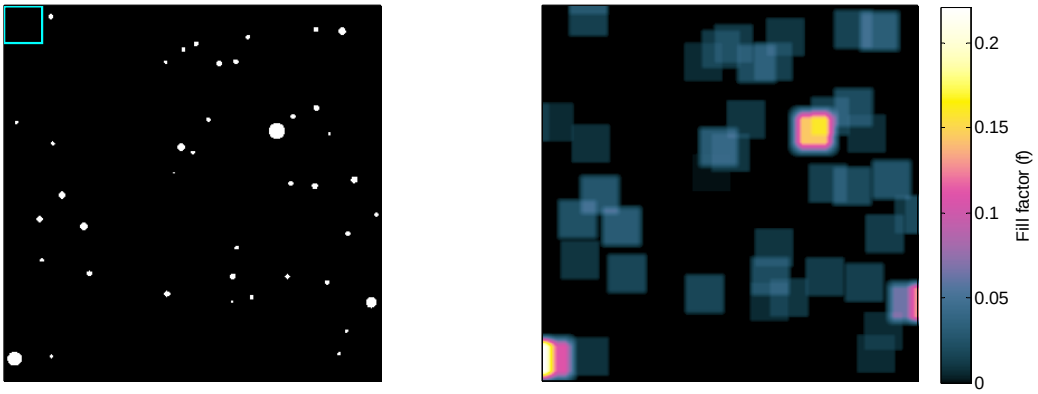


**Fig. A1.** Simulation 1 (case 1): (left) value of $f$ for each pixel on the simulated surface. The sensor *FOV* (blue box, 1/10$^{th}$ the linear dimension of the image) moves over the contaminated surface. (right) The fill factor as seen by the *FOV* for the contaminated surface. The likelihood for the sensor *FOV* to encounter contamination is $P(H_1)$=0.4.

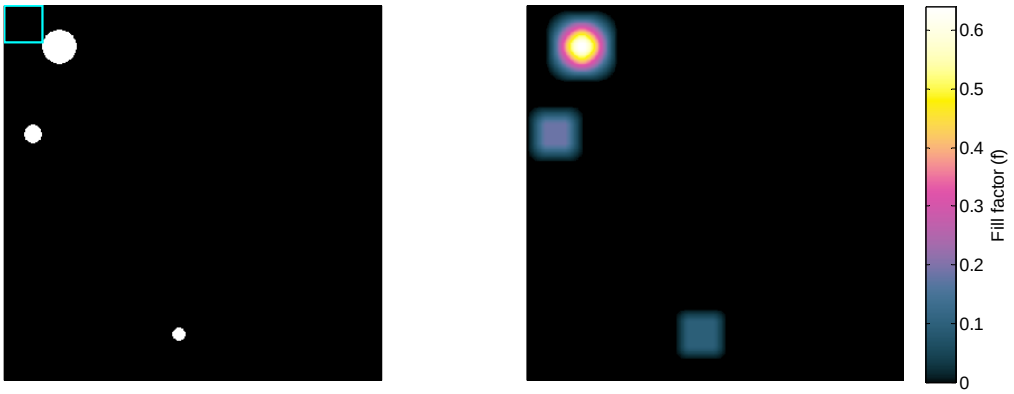


**Fig. A2** Simulation 2 (case 2): same as Fig. A1 except that individual contamination events are larger in cross-sectional area; it takes fewer events for the same total area of contamination. The likelihood for the sensor *FOV* to encounter contamination is $P(H_1)$=0.072.

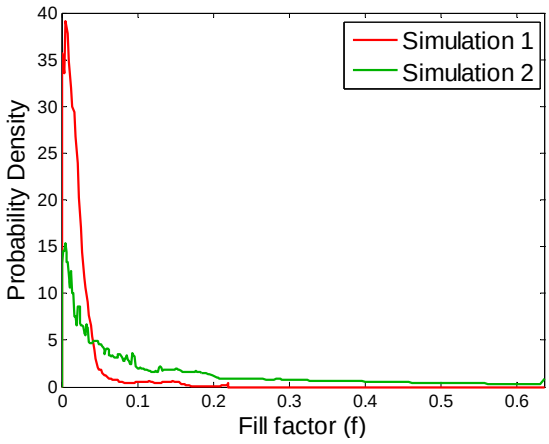


**Figure A3.** Fill factor probability for simulations in Fig A1 and A2.

## References

1. A. Ben-David, and C. E. Davidson (2013). "Radiative transfer model for contaminated rough surfaces," ECBC-TR-1084, U.S. Army, Edgewood Chemical Bilogical Center, Aberdeen Proving Ground, MD.

2. S. M. Kay, (1998). *Fundamentals of statistical signal processing*, Detection theory, Prentice Hall PTR: Upper Saddle River, NJ.

3. M. I. Skolnik, (2001). *Introduction to radar systems, 3rd edition*, McGraw-Hill, New York, NY.

4. M. A. Richards (2005). *Fundamentals of radar signal processing, 1st edition*, McGraw-Hill, New York, NY.

5. N. Hagen, R. T. Kester, L. Gao, and T. S. Tkaczyk, (2012). "Snapsot advantage: a review of the light collection improvement for parallel high-dimension measurement," Optical Engineering, **51**, p111702-111707.

6. R. Kunz, M. Aernecke, M. Clark, C. Wynn, and K. Gregory (2013). "Final report for trace explosive signature studies," ECBC-CR-131, U.S. Army, Edgewood Chemical Bilogical Center, Aberdeen Proving Ground, MD.

7. P. Bhattacharyya and B. K. Chakrabati (2008). “The mean distance to the *n*th neighbour in a uniform distribution of random points: an application of probability theory”, *Eur. J. Phys.* **29,** p639-6344.

8. A. Ben-David and C. E. Davidson (2012). “Probability theory for 3-layer remote sensing radiative transfer model: univariate case”, Opt. Express, **20**, p1004-1033.

9. C. Richmond (1996). “Derived PDF of maximum likelihood signal estimator which employs an estimated noise covariance,” IEEE Transaction on Signal Processing, 44, p305-315.

10. J. Han, P. K. Varshney, and R. Srinivasa, (1993). “Distributed binary integration,” IEEE Transaction on Aerospace and Electronic Systems, AES-**29**, p2-8.


EDGEWOOD CHEMICAL BIOLOGICAL CENTER
A U.S. Army RDECOM Laboratory